Calibration of the Hopkins Ultraviolet Telescope

Jeffrey W. Kruk[1]

Abstract

The Hopkins Ultraviolet Telescope (*HUT*) flew aboard the space shuttle Columbia during the Astro-1 mission in December, 1990. *HUT* has been optimized for obtaining spectrophotometric observations of faint objects at wavelengths ranging from the Lyman limit (912Å) up to 1860Å. The telescope layout is shown in Figure 1, and the instrument parameters are given in Table 1. Calibrations were performed pre-flight, in-flight, and post-flight. These calibrations are described below.

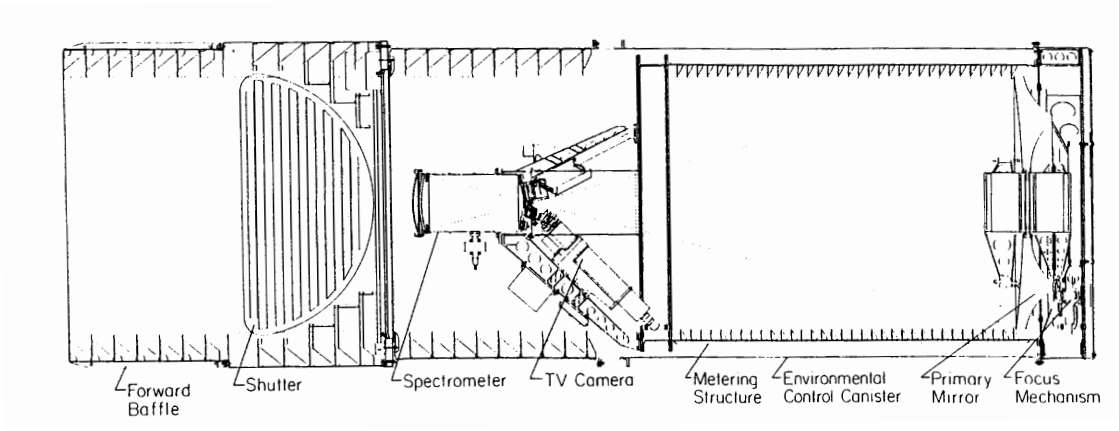

Figure 1: *HUT* layout

I. Pre-Flight Calibration

The pre-flight calibration consisted of separate measurements of the reflectivity of the primary mirror and spectrograph throughput, since the large size of the telescope precluded a laboratory calibration of the instrument as a whole. The primary mirror reflectivity was determined at 8 wavelengths at numerous points over its surface, by comparing its reflectivity at each point with that of an iridium coated test flat whose reflectivity was measured in a conventional reflectometer. The primary mirror reflectivity was subsequently monitored with iridium coated witness mirrors which accompanied the primary mirror at all times. The spectrograph throughput was measured at 29 wavelengths and at 19 entrance angles distributed over the f/2 cone of the telescope. The incident fluxes were determined using both a microcline plate detector and an EMR G tube which were calibrated against photodiodes which in turn were calibrated at NIST. The resulting pre-flight determination of the effective area for first order wavelengths is shown in Figure 2a.

1. CAS, Johns Hopkins University, Baltimore, MD 21218

Table 1: *HUT* Instrument Characteristics

Telescope	
Prime Focus Paraboloid	
Aperture	0.9 m
Focal Ratio	f/2
Plate scale	8.727 microns/arc sec
Mirror Coating	Iridium
Aperture Door Areas	5120, 2560, 50, 1 cm**2
Spectrograph	
Rowland Circle Mounting	
Grating Diameter	200 mm
Radius of Curvature	400 mm
Grooves	600 l/mm, holographic
Coating	Osmium
Spectral Resolution	3Å
Wavelength Coverage	830–1860Å, 415–930Å
Scattering	$1x10^{-5}$ per Å
Detector	
Open Window Microchannel Plate Intensifier	
Photocathode	Cesium Iodide
MCP's	two 80:1 L/D, 10 pores, 15 degree bias
Anode	Phosphor screen with photodiode readout
Active Length	25 mm
Diode Size	25 μm x 2.5 mm
Time Resolution	1 msec
Background	$7.7x10^{-4}$ counts/sec/Å
Electron Repeller Grid	95 percent Transmission, 20 l/inch

A mercury lamp mounted on the spectrograph provided a rough monitor of the throughput over the two years prior to the flight. The observed count rate from the lamp declined steadily by about 25 percent over this period, and both in-flight and post-flight calibrations give a throughput 20-30 percent below the pre-flight calibration. The observed rate from the lamp has been stable since the flight, indicating that the post-flight calibration should be representative of the actual in-flight sensitivity. These results are consistent with our experience for CsI photocathode aging. The ratio of the post-flight to preflight calibrations is shown in Figure 2b.

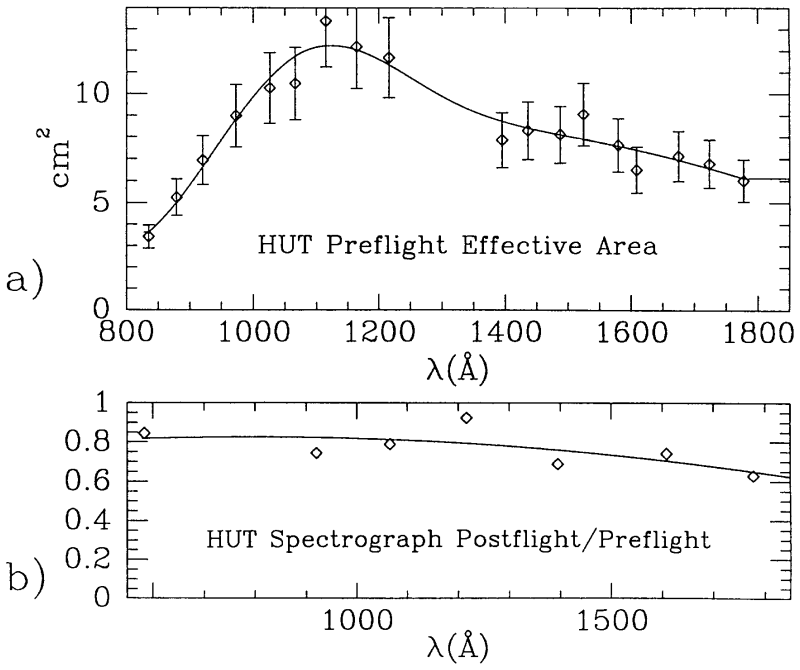

Figure 2: a) preflight calibration; b) ratio of post/pre flight calibrations.

II. In-Flight Calibration

Our first order flux calibration is defined by the model atmosphere for the DA white dwarf G191-B2B of P. Bergeron. The model parameters T_{eff} = 59,250 K and log g = 7.5 were determined from observations at visual wavelengths (Holberg et al., 1991).

The raw spectrum is corrected for phosphor persistence (7.3 percent), detector dark count (0.01–0.1 percent), detector deadtime (5 percent at peak of spectrum), and second and third order flux (≤ 3 percent). The model itself is corrected for transmission through the interstellar medium ($N_H = 1.7 \times 10^{18}$ cm^{-2}, b = 10 km/s). Uncertainties in the proper effective temperature lead to changes in our effective area of less than 5 percent, to within a few angstroms of the Lyman edge. The resulting flux-calibrated spectrum and the model spectrum are shown in Figure 3. The apparent absorption feature at 1600Å is a detector defect and the peak at 1216Å is contamination from airglow. Other small deviations of the spectrum from the model are due to the requirement that our effective area curve vary smoothly with wavelength.

A test of the model dependence of the calibration can be made by comparison with a different model atmosphere. Our adopted flux for G191-B2B and the model atmosphere of D. Coaster are shown in Figure 4, for 900–1140Å (the two models give essentially identical results longward of 1100Å). The only appreciable differences between the models occur between the strong Lyman β, γ, and δ absorption lines, due to differences in the treatment of pressure broadening.

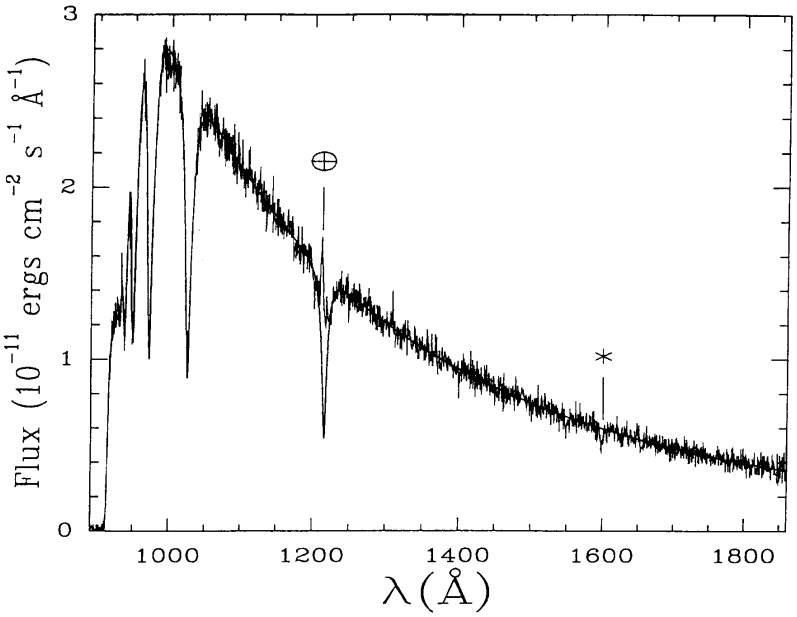

Figure 3: Comparison of HUT spectrum of G191-B2B with model from P. Bergeron.

An additional test of the calibration is provided by comparing the observed spectrum of the white dwarf HZ43 with the Koester model for this star. All parameters in this model were determined by observations made at visual wavelengths. The *HUT* spectrum has been multiplied by 1.08 to account for pointing jitter. The *HUT* spectrum and the model are shown in Figure 5. The peaks seen at 1216 and 1304Å are due to airglow. No systematic disagreements greater than a few percent are seen longward of about 975Å. Shortward of 975Å the data falls as much as 15 percent below the model, which may reflect slight errors in the adopted temperatures of HZ 43 or G191-B2B, or may be due to differences in modelling absorption by the converging Lyman series in the presence of severe pressure broadening.

Calibrations for the various aperture door configurations were obtained by observing suitable stars through multiple doors.

III. Post-Flight Calibration

The post-flight calibration of the spectrograph was performed one year after the mission. We repeated the pre-flight spectrograph calibration at a subset of wavelengths and angles, and multiplied by the pre-flight mirror calibration to obtain the effective area. The results are shown in Figure 6, along with the in-flight effective area calibration. While fluctuations of up to 10 percent are seen, the mean ratio differs from unity by less than 1 percent. This agreement is fortuitously good, given that the uncertainties in the calibration of the NIST photodiodes used in the laboratory measurements are greater than this.

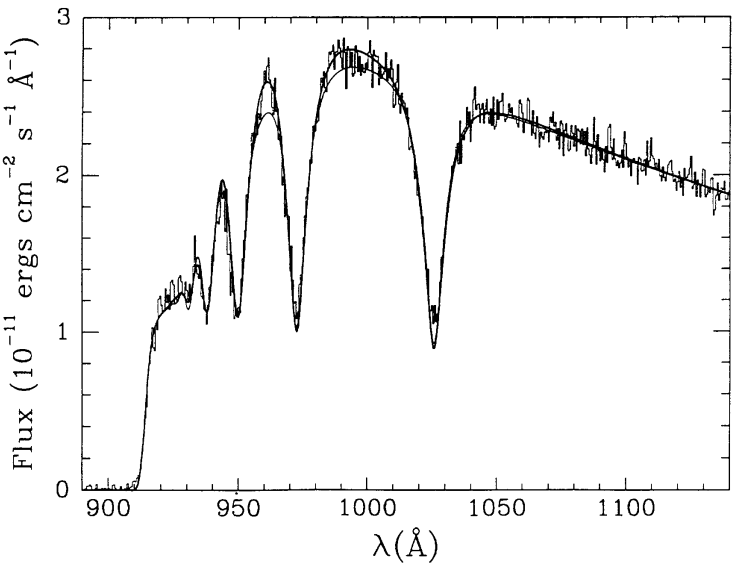

Figure 4: Comparison of adopted flux for G191-B2B with model from D. Coaster.

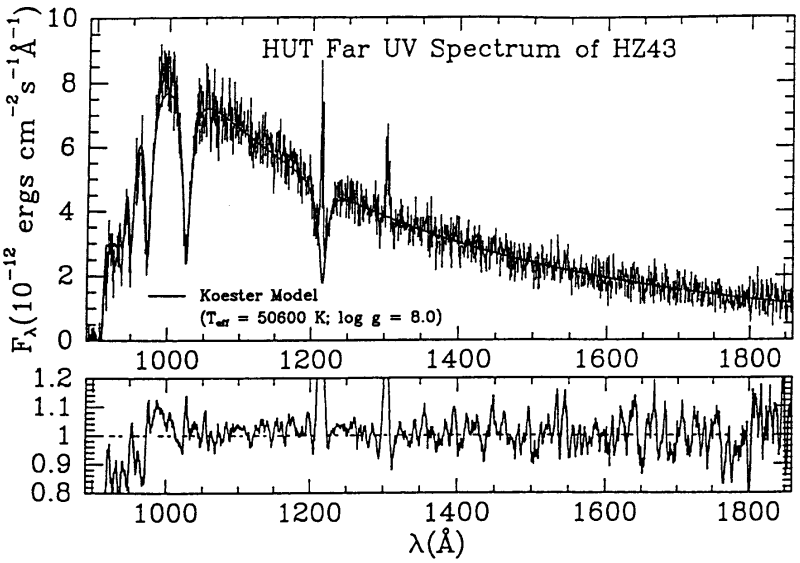

Figure 5: Comparison of *HUT* spectrum of HZ43 with model from Koester.

We recently gained access to the primary mirror and measured its reflectivity at 1236Å. It is unchanged from its pre-flight value of 19 percent. A more detailed measurement of the mirror reflectivity will be performed when it is shipped back to JHU.

We also performed a post-flight spectrograph calibration at SURF. There were two aspects to this calibration: determining the detector response to a flat field, and determining the absolute spectrograph efficiency.

The flat field measurements revealed two types of features: shadows cast by the wires of the electron repeller grid, and a defect in the detector in the vicinity of pixel 1510 (corresponding to 1600Å in the first order spectrum). The dip at about pixel 760 is caused by reduced gain in the microchannel plates where they were illuminated by the intense geocoronal Lyman alpha radiation. A typical spectrum obtained at a single entrance angle is shown in Figure 7.

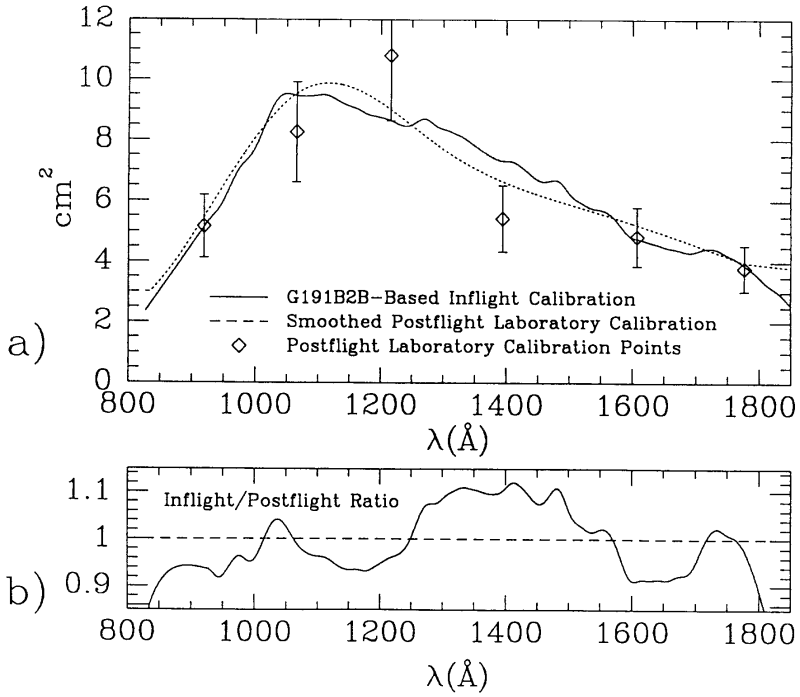

Figure 6: Comparisons of in-flight and post flight calibrations.

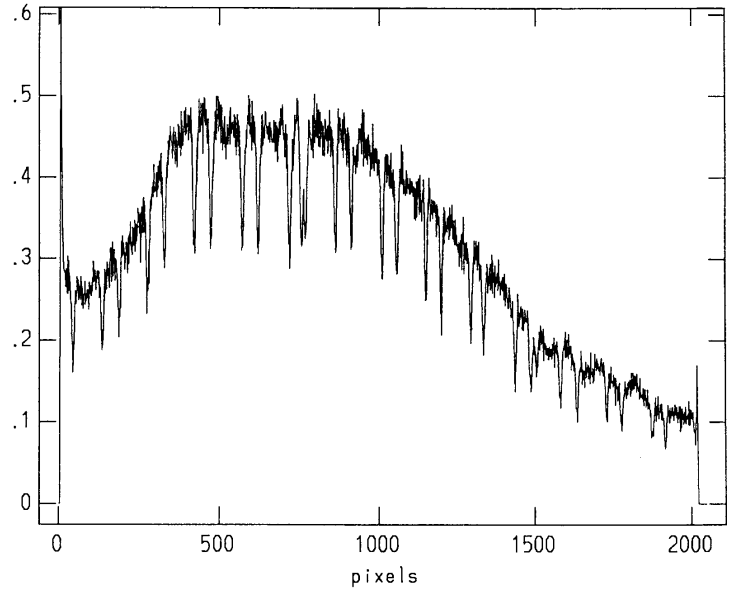

Figure 7: Flat field taken at a single entrance angle, note the effect of the wires of the electron repeller guide on the flat field.

The wire shadows are effectively smoothed out by the f/2 beam obtained for observations made through the large telescope doors, but not by the f/20 beam produced by the 50 cm^2 door. A correction for this effect was determined by measuring the spectrograph response at 26 entrance angles distributed evenly over this f/20 cone. The resulting average is shown in Figure 8. A smooth curve was fit to the dips in this average spectrum to serve as a flat field correction for all observations made through the 50 cm^2 door. This correction was tested by coadding spectra of three hot stars observed by both *HUT* and *IUE*, and comparing the ratio of the *HUT*

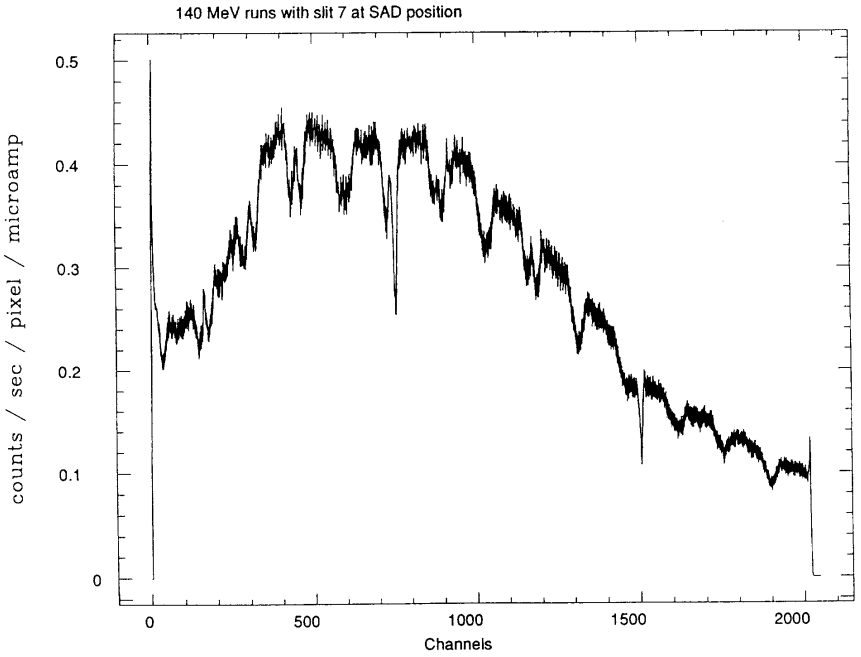

Figure 8: Average flat field as described in text.

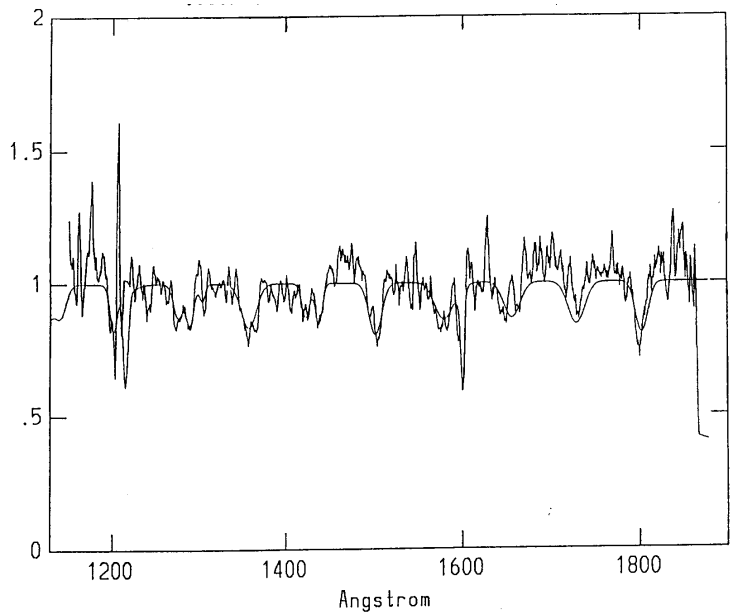

Figure 9: Comparison of the ratio of *HUT* to *IUE* observations with proposed correction for flat field features.

to *IUE* spectra with the proposed correction. The agreement is quite good, as can be seen in Figure 9.

The efficiency calibration was complicated by the fact that the spectrograph has measurable sensitivity through the first 4 diffraction orders. At the normal SURF beam energy of 284 MeV the flux rises with decreasing wavelength about as fast as our grating efficiency falls, with the result that the observed count rates were

comparable in all four orders. In normal operation the flux is cut off at 912Å by the interstellar medium, but no such filter is available at SURF! Attempts to run at four different beam energies and solve directly for the spectrograph efficiency in the first four grating orders were not successful. However, data taken at a beam energy of 100 MeV had sufficiently little flux in our higher order bandpass (2-3 percent of first order) to be easily modelled and subtracted. Since the synchrotron had never been run at 100 MeV, the potential systematic errors are difficult to assess. We attempted to account for these by obtaining a second calibration at the usual beam energy of 284 MeV through cross-calibrated magnesium fluoride and calcium fluoride filters. This produced a calibration useful longward of 1260Å, which was used to fix the beam energy and orbital plane tilt of the 100 MeV data. Due to limitations in available beam time we only took such data at the center of the grating. We multiplied these data by a smooth fit to the ratio of grating average to grating center sensitivity obtained at fixed wavelengths in the JHU calibration facility. This result is shown in Figure 10, along with the in-flight determination of the spectrograph efficiency (calculated by dividing the in-flight effective area curve by the pre-flight measurements of the primary mirror effective area). These two calculations generally agree to within a few percent, with occasional disagreements of up to 7 percent. The discrepancy does grow below the Lyman edge, (to about 20 percent at 830Å, where we have no in-flight calibration data. The sharp peaks seen at either end of the spectrum are due to mis-centroided events at the edge of the detector active area. The ripples seen in the SURF data are due to the fact that the long slit used in the measurement shown does not smooth out the shadows cast by the repeller grid as effectively as the f/2 beam of the full telescope.

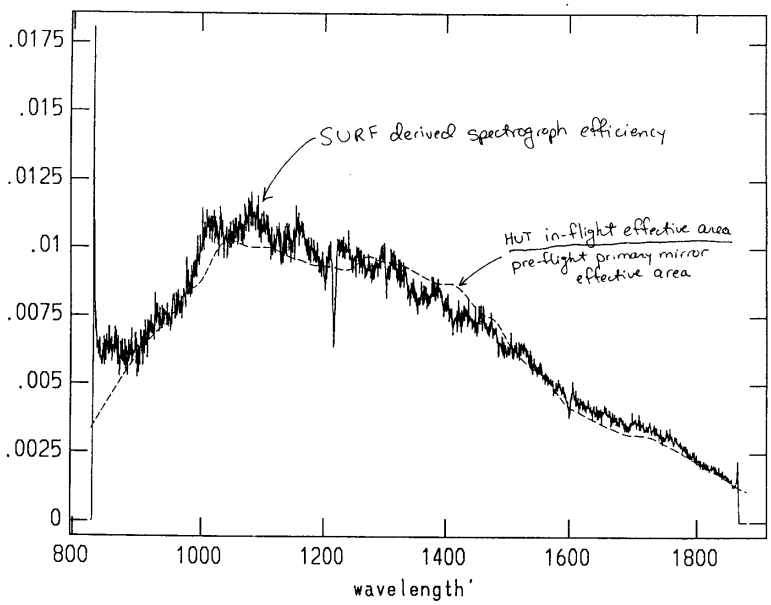

Figure 10: SURF calibration

IV. Comparison with Other Instruments

Figure 11 shows spectra of G191-B2B from *HUT*, *IUE*, and Voyager. The agreement is quite good, apart from broad undulations in the *IUE* spectrum of up to 10 percent. These undulations are inherent in the old *IUE* calibration used in this plot; they

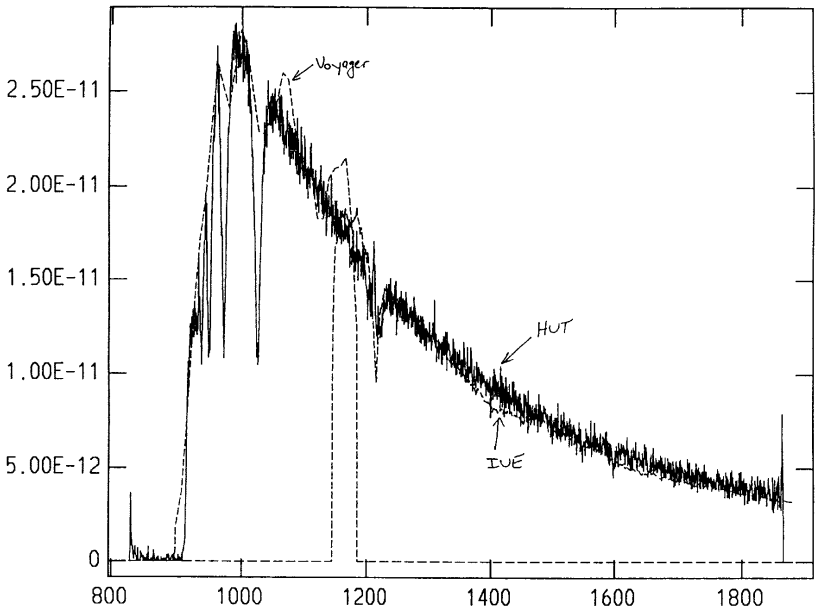

Figure 11: Spectra of G191-B2B from *HUT*, *IUE* and Voyager.

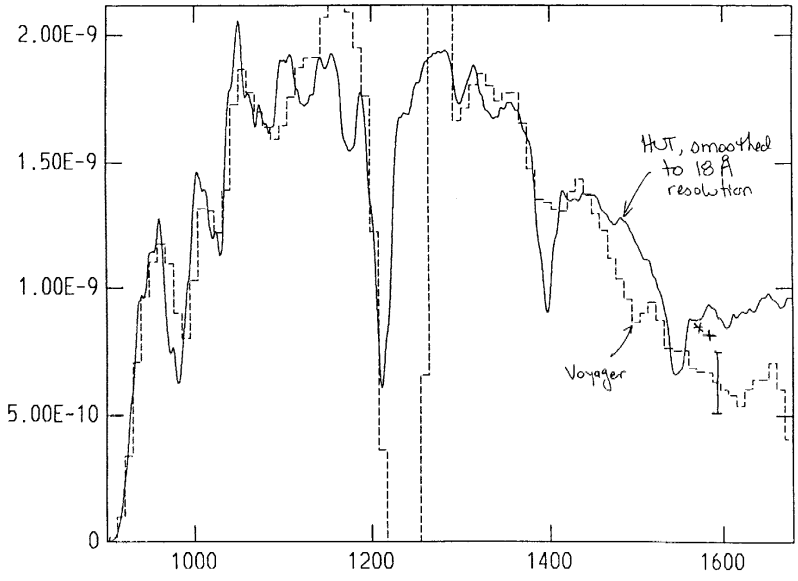

Figure 12: Spectra of π Agr from Voyager and *HUT*.

would disappear if the new *IUE* calibration had been used. Figure 12 shows spectra of πAqr from Voyager, and from *HUT* (after smoothing to match the Voyager resolution). The agreement is again excellent.

V. Conclusion

The absolute first order sensitivity of *HUT*, as defined by the model atmosphere for G191-B2B, is in agreement with post-flight laboratory calibrations to within the 10 percent uncertainty of the laboratory data. Different atmosphere models disagree, typically by about 5 percent, for wavelengths below 1000Å. This is due in part to the

extreme sensitivity of the flux at these wavelengths to small changes in the effective temperature, and in part to difficulties in modelling line broadening effects in the vicinity of the converging Lyman series. The Astro-2 guest investigator program of Dave Finley will address this problem. The *HUT* laboratory calibration should help resolve the controversies that have existed shortward of Lyman α, where various instruments have disagreed by factors of as much as 4 to 6 (Holberg et al. 1991, and references therein). Several refinements of our calibration procedures are planned for the Astro-2 mission, which should enable us to improve upon the accuracy obtained for Astro-1.

References

Holberg et al., ApJ 375, 716 1991.